Mature 137-Registry Carriers and Particle-Like Excitations in an Open-Token Distinction Engine

Jason Merwin
Independent Researcher

Draft of April 30, 2026

Abstract

A prior distinction-engine construction recovered a 137-object registry at DAG size 7 and partitioned it into sectors of $81 + 40 + 16$, aligning with the spatial, interface, and gravitational sectors proposed in Relational Mathematical Realism. The present manuscript consolidates two subsequent analyses. First, we study mature registry carriers: larger relational objects that contain the full 137-type registry as an embedded motif. Exact DAG-size joins and 137-bit registry signatures recover DAG-8, DAG-9, and DAG-10 layers while compressing motif state space by factors of 6.85×, 20.43×, and 46.01×. Minimal full-registry carriers have DAG size 309. Eight non-isomorphic carrier histories preserve the same condensable typed mediation geometry: 72 spatial nodes, 38 interface nodes, 16 gravitational nodes, and 288 mediated S–G edges per condensable interface node. Typed dynamics lifted onto these mature carriers show no statistically detectable topology effect on interface-enabled condensation. A screening audit identifies full binary S–G conflict deletion as the wild-type interface rule, producing $S_{\mathrm{DYN}} \simeq 9.61$, $S_{\mathrm{OFF}} \simeq 2.04$, and a 4.73× dynamic/OFF enhancement. Loss-of-function tests identify the true invariant as complete I-mediated coverage of the active S–G conflict graph: the 38 condensable I nodes split into two complementary 19-node half-covers, each covering 288 of 576 active S–G edges.

Second, we extend the analysis to an open-token distinction engine, in which finite type identity is separated from lineage-distinct token identity. The type-guarded open-token process preserves the canonical 137 DAG-7 type layer exactly while allowing unbounded token multiplicity. Particle-detector tests on open-token dynamics recover robust K3/baryon-like candidates: five stable candidates with $k3\_score = 1.0$, high closure, and fixed carrier support. I-cage/lepton-like structures appear as suggestive precursors, including a high-scoring cage-localized candidate, but not yet as fully closed localized leptons. These results support a layered interpretation: the DAG-7 registry is a finite reusable type grammar; DAG-309 carriers are mature local embeddings of that grammar; and open-token dynamics permit stable particle-like excitations over repeated registry instances. We identify a mathematically natural route from distinction-generated registry types to mature carriers and K3-centered particle-like object.

1 Introduction

Relational Mathematical Realism (RMR) proposes that physical structure may be modeled as a finite typed relational registry rather than as fields on a pre-existing continuum. Earlier work derived a 137-element registry and connected it to a sector decomposition of $81 + 40 + 16$ elements, interpreted as spatial/substrate, interface, and gravitational sectors [3, 8]. A separate distinction-engine construction later recovered the same 137-object registry and the same partition from a primitive relational operation, providing a bottom-up logical route to the same architecture [11].

This convergence suggests that the registry is not merely a fitted numerical scaffold, but a recurrent relational-combinatorial structure.

The present paper addresses the next object-level question. If a 137-type registry exists as a local grammar, what does it mean for that grammar to be embedded in larger relational objects? Does the typed dynamics depend on the historical assembly of the embedding carrier, or is the relevant physics intrinsic to the registry's S–I–G mediation tensor? And once an open population of lineage-distinct tokens is allowed, do stable particle-like excitations appear?

The resulting picture has three layers:

1. A finite type grammar: the DAG-7 137-object registry with sectors $81 + 40 + 16$.
2. Mature carriers: DAG-309 objects that embed the full registry as lineage history while preserving the typed mediation tensor.
3. Open-token excitations: repeated lineage-distinct instances of registry types supporting localized K3/baryon-like and I-cage/lepton-like candidate patterns.

The main result is that carrier history is largely irrelevant once typed mediation coverage is preserved. What matters is not the passive merge tree but the coverage of the S–G conflict graph by the I-sector. This provides a natural bridge from abstract registry derivation to particle-like object formation.

Relation to computational and mathematical-universe programs

The present construction also sits within a broader class of approaches in which physical structure is not assumed to be fundamental continuum substance, but is instead understood as the emergent behavior of an underlying formal or computational system. Wolfram's program emphasizes that simple discrete rules can generate unexpectedly rich structures, including persistent localized patterns, causal networks, and large-scale regularities that need not be inserted by hand [13]. Tegmark's mathematical-universe hypothesis, by contrast, places the emphasis on the ontological status of mathematical structure itself, proposing that physical existence may ultimately be identified with mathematical existence rather than merely described by mathematics [15].

The distinction-engine framework developed here is sympathetic to both perspectives, but it is more specific in its present claim. It does not assume that arbitrary computational rules are physically realized, nor does it require the full ontological commitment that all mathematical structures exist physically. Instead, the evidence presented here concerns a particular relational construction: a two-primitive distinction process that recovers a finite 137-object type registry, admits mature DAG-309 carriers embedding that registry, and supports open-token excitations over repeated lineage-distinct registry instances. In this sense, the registry functions as a local algebraic grammar rather than as a universal cellular automaton or an unrestricted mathematical ensemble.

This distinction is important for the interpretation of the particle-like results. The open-token engine does not merely generate complexity; it preserves a closed type layer while allowing token multiplicity, thereby separating local grammar from extended population. The candidate K3/baryon-like and I-cage/lepton-like structures are therefore not claimed as arbitrary emergent patterns in a generic discrete system, but as localized excitation patterns over a recovered finite registry. The relevant question is consequently narrower and more testable: whether this specific registry grammar, when embedded in mature carriers and opened to repeated token instances, supports stable object-like excitations with reproducible topological signatures.

2 Background: the DAG-7 registry

The distinction engine begins with two primitive objects. Each distinction operation joins an unordered pair of existing objects into a new composite whose ancestry DAG contains both parents and the new object. The DAG size of an object is the number of distinct objects in its ancestry, including itself. In the canonical engine with two primitives, unordered pairs, and no self-pairing, DAG size 7 contains exactly 137 objects [11].

The executable partition used here is

$$S = \{x : parentOverlap(x) \leq 3\}, \tag{1}$$
$$G = \{x : parentOverlap(x) > 3 \text{ and } m(x) = 8\}, \tag{2}$$
$$I = \{x : parentOverlap(x) > 3\} \setminus G, \tag{3}$$

where $m(x)$ is a shape-multiplicity class within DAG-7. This yields

$$|S| = 81, \qquad |I| = 40, \qquad |G| = 16. \tag{4}$$

The overlap graph on the 137 DAG-7 registry nodes connects two nodes when their ancestry overlap exceeds 3. It contains a universal core of 11 nodes, partitioned as 9 spatial and 2 interface nodes. Excluding these universal nodes leaves a condensable dynamical substrate of

$$|S_c| = 72, \qquad |I_c| = 38, \qquad |G| = 16. \tag{5}$$

The original typed simulator found that the interface sector enables matter-like S-sector condensation: freezing I off suppresses S realization, whereas dynamic I or frozen-on I raises S realization to a much larger value. The mature-carrier analysis below asks whether this effect survives embedding in larger carrier histories.

3 Exact motif-aware generation beyond DAG-7

Naive distinction-engine enumeration becomes rapidly infeasible beyond DAG-7. The mature-carrier analysis replaces global step-space enumeration with exact DAG-size joins. If A_x is the ancestry set of object x, then a child $c = d(a, b)$ has size

$$|A_c| = |A_a \cup A_b| + 1 = |A_a| + |A_b| - |A_a \cap A_b| + 1. \tag{6}$$

Therefore, to generate target DAG size L from parent sizes p_a, p_b, parent pairs must satisfy

$$|A_a \cap A_b| = p_a + p_b + 1 - L. \tag{7}$$

Each object also receives a 137-bit registry signature

$$\sigma(x)_i = 1 \iff A_{r_i} \subseteq A_x, \tag{8}$$

where r_i is the ith DAG-7 registry object. The signature recurrence is

$$\sigma(d(a, b)) = \sigma(a) \vee \sigma(b). \tag{9}$$

Objects with identical registry signatures may be collapsed for motif statistics even when their exact ancestry rows are retained for exact joins.

This method exactly recovers DAG-8 = 945, DAG-9 = 7927, and DAG-10 = 78731 objects. The number of distinct motif signatures is much smaller: 138, 388, and 1711. Thus the compression ratios are 6.85×, 20.43×, and 46.01×, respectively (Fig. 1).

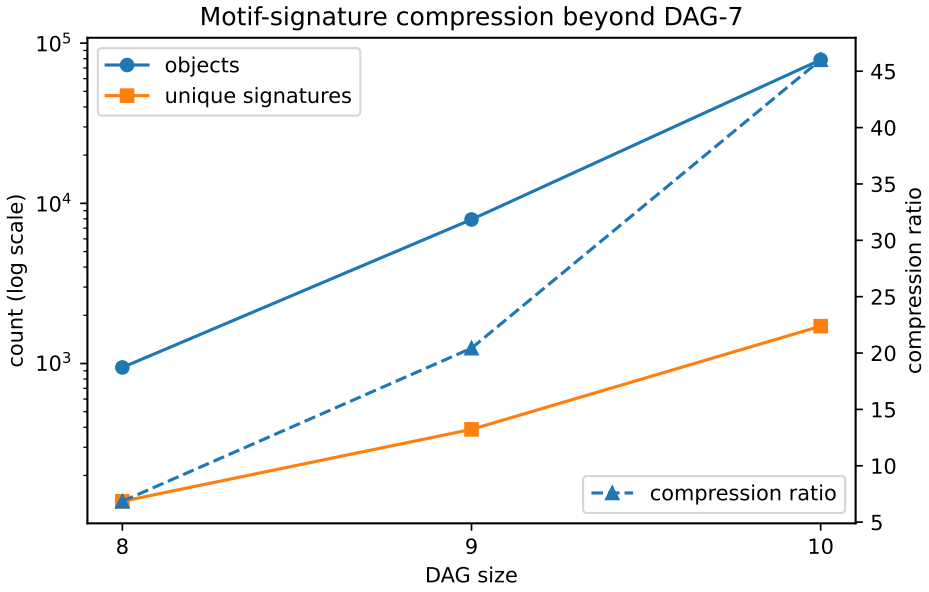

Figure 1: Exact DAG-size generation and motif-signature compression. Object counts grow from 945 at DAG-8 to 78,731 at DAG-10, while unique 137-bit registry signatures grow from 138 to 1711. The registry-footprint state space compresses far faster than the full object space.

4 Minimal full-registry mature carriers

Let R denote the 137 DAG-7 registry nodes. The union of their DAG-7 ancestries contains 173 seed objects. A binary merge tree over 137 leaves adds 136 new merge nodes, so a minimal carrier containing all registry leaves has DAG size

$$L_{\min}(R) = 173 + 137 - 1 = 309. \tag{10}$$

Across any minimal full carrier, the total parent-overlap sum is conserved. If $o_t = |A_{a_t} \cap A_{b_t}|$ is the overlap at merge t, then

$$309 = 137 \cdot 7 + 136 - \sum_{t=1}^{136} o_t, \tag{11}$$

so

$$\sum_{t=1}^{136} o_t = 786, \qquad \bar{o} = 786/136 = 5.779411\ldots. \tag{12}$$

Eight carrier histories were generated: maximum-overlap, minimum-overlap, balanced maximum-overlap, cross-sector-first, two sector-staged policies, a G7 degree-weighted policy, and a random policy. Weisfeiler–Lehman hashes and exact typed isomorphism tests show that these upper merge trees are non-isomorphic. Nevertheless, the final typed mediation geometry is invariant: each carrier contains 72 condensable S nodes, 38 condensable I nodes, 16 G nodes, and exactly 288 mediated S–G edges per condensable I node.

5 Typed dynamics on mature carriers

The mature-carrier lift treats only the 137 registry leaves as typed dynamical degrees of freedom. The 136 anonymous merge nodes act as passive carrier structure. The typed degrees of freedom remain:

- S nodes: ternary states $s \in \{-1, 0, +1\}$ with moves $0 \leftrightarrow \pm 1$.
- G nodes: binary states $g \in \{-1, +1\}$, always realized.
- I nodes: relational channels $i \in \{0, 1\}$ that screen S–G conflict when active.

The energy includes S realization, S–S conflict, G–G conflict, S–G conflict, S saturation, and I activation cost. A screening audit compared multiple S–G mediation rules. The wild-type operator is full binary S–G conflict deletion:

$$J_{SG}^{\text{eff}}(s, g) = \begin{cases} J_{SG}, & \sum_i I_i M_{i,s,g} = 0, \\ 0, & \sum_i I_i M_{i,s,g} > 0. \end{cases} \tag{13}$$

Under this rule, dynamic I produces $S_{\text{DYN}} = 9.6145$, while I-off produces $S_{\text{OFF}} = 2.0361$, a dynamic/OFF enhancement of $4.7276\times$. Across eight non-isomorphic carriers, one-way ANOVA gives $p = 0.4368$, indicating no statistically detectable carrier-history effect (Fig. 2).

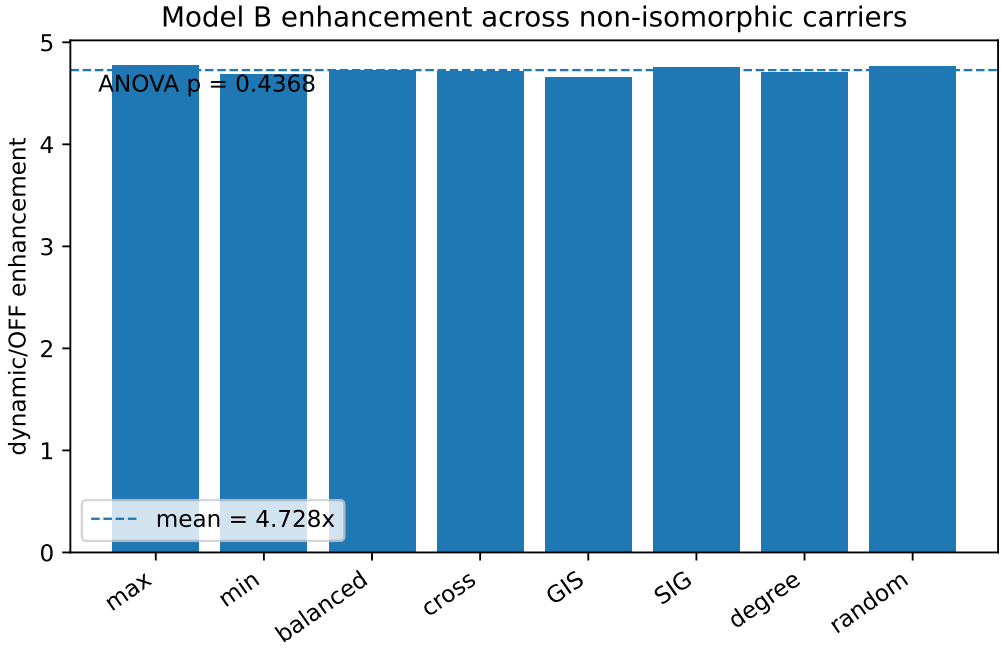

Figure 2: Model B enhancement across non-isomorphic mature carriers. The full-binary screening operator produces a dynamic/OFF enhancement near $4.73\times$ across eight carrier histories. The plotted values are regenerated from summary values; original mature-carrier figures may be substituted if available.

6 Mutagenesis and the two-key interface cover

Mutagenesis showed that the carrier does not depend on fragile active-site identity. Swapping two universal I identities with two deep non-universal S identities did not attenuate enhancement. Transposing five G identities with five deep S identities also preserved function. A max-antagonism carrier that changed passive backbone folding preserved the mediation tensor and the condensation phenotype.

Loss-of-function tests identified the true control variable: complete coverage of the S–G conflict graph. The 38 condensable I nodes split into two complementary groups of 19 nodes. Each group covers 288 of the 576 active S–G edges; their union covers all 576:

$$I_c = I_A \cup I_B, \qquad |I_A| = |I_B| = 19, \tag{14}$$

$$cover(I_A) = cover(I_B) = 288, \qquad cover(I_A \cup I_B) = 576. \tag{15}$$

Small I-node knockouts preserve function when coverage remains complete. When coverage falls to 50%, the system enters a damaged intermediate phenotype. When coverage is eliminated, enhancement collapses to OFF-like behavior (Fig. 3).

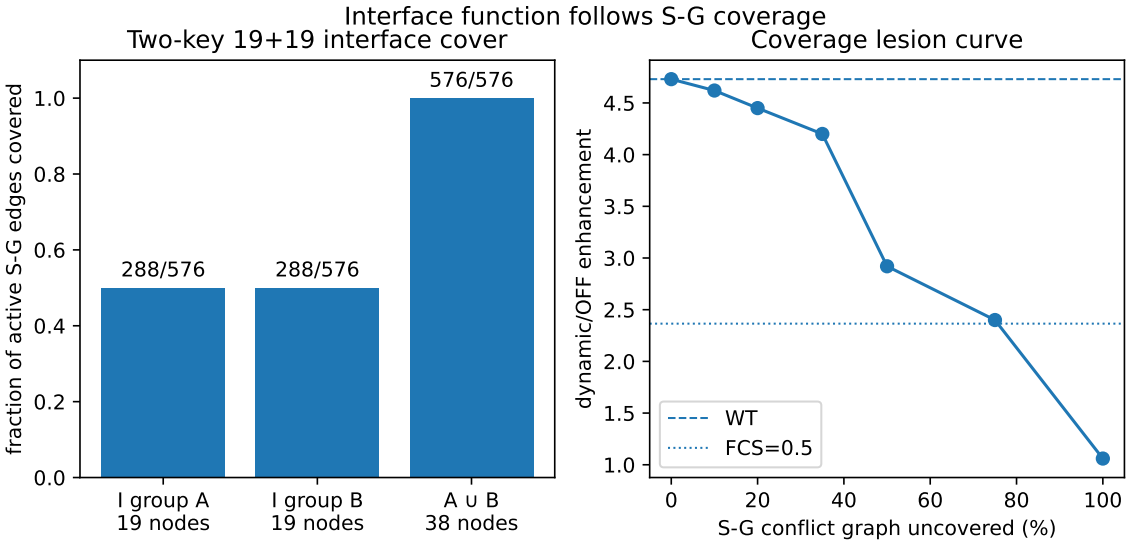

Figure 3: The functional invariant is I-mediated S–G coverage. The 38 condensable I nodes form two 19-node half-covers, each covering 288 of 576 active S–G conflict edges. Direct coverage lesion produces graded loss of function.

7 Type closure and token openness

A finite distinction engine appears, at first, to be incompatible with an extended universe. The resolution is to distinguish type identity from token identity. The closed distinction engine is a type-level quotient: it discovers the finite local grammar. A physical token may have the same type as another token but remain distinct by lineage, embedding, or causal neighborhood:

$$\tau(x) = \tau(y), \qquad \lambda(x) \neq \lambda(y) \quad \Longrightarrow \quad x \neq y, \tag{16}$$

where τ denotes abstract type and λ denotes lineage or embedding history.

The type-guarded open-token engine permits repeated lineage-distinct tokens while requiring productive novelty to use distinct parent types. This process generated 19,530 tokens by tick 5, but the DAG-7 type layer contained exactly the canonical 137 registry types and no extras. By contrast, a fully token-distinct rule generated 26,796 tokens and 201 DAG-7 types, preserving the canonical registry as a subset but adding 64 extra DAG-7 types (Table 1; Fig. 4).

Table 1: Open-token distinction engine compared to the closed type quotient. The type-guarded open engine preserves the canonical DAG-7 layer exactly while allowing token multiplicity.

Model	Tokens	Unique types	DAG-7 types	Canonical recovered	Extra DAG-7 types
Closed type quotient	–	173	137	137	0
Open, type-guarded	19,530	2,280	137	137	0
Open, token-distinct	26,796	3,626	201	137	64

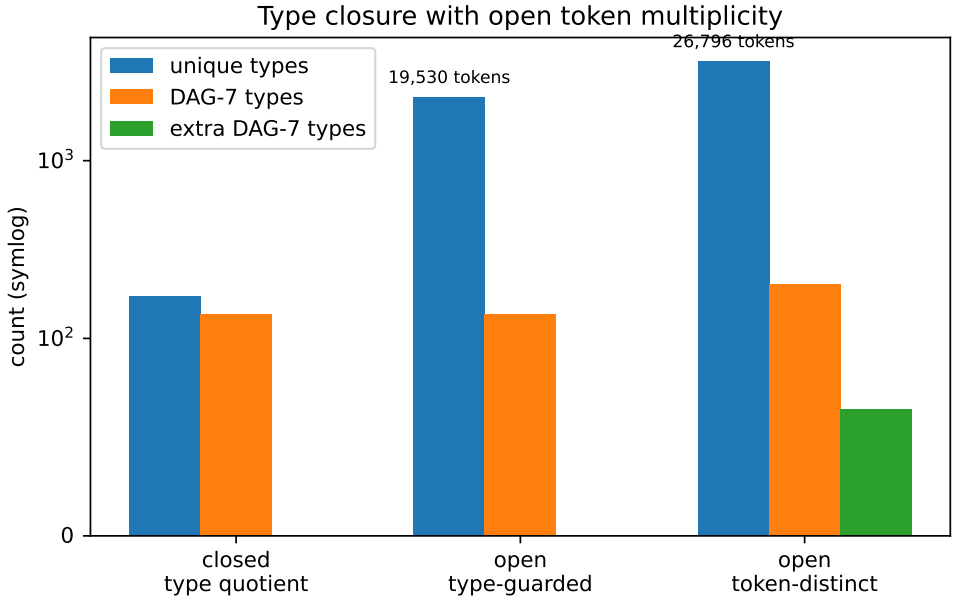

Figure 4: Type closure with open-token multiplicity. The type-guarded open-token process expands the token population while preserving the canonical 137 DAG-7 type layer exactly.

Thus the registry is unique as a type and repeatable as a token. The finite DAG-7 registry is not the count of physical objects; it is the reusable local algebraic grammar. Extended relational spacetime is modeled as an open population of lineage-distinct carrier tokens whose type projection remains finite.

8 Open-token particle search

Having established mature carriers and token openness, we next ask whether open-token dynamics support localized particle-like excitations. The open-token engine instantiates registry types as lineage-distinct tokens on carriers. The particle detector scores candidate structures by persistence, locality, closure, carrier support, K3 score, photon score, mass score, lepton score, baryon score, and

gauge score. The relevant particle endpoints are K3/baryon-like candidates and I-cage/lepton-like precursors.

8.1 Baryon-like K3 candidates

The baryon seed experiment produced five baryon candidates. All five had $k3\_score = 1.0$, fixed carrier support of three, zero centroid switches, zero hop rate, high closure scores near 0.96, and baryon scores between approximately 2.78 and 2.84 (Table 2; Fig. 5). Their centroid paths remain localized on a fixed carrier, consistent with stable K3-centered excitation.

Table 2: Summary of five K3/baryon-like candidates from the open-token baryon seed experiment.

Candidate	Carrier support	K3 score	Closure	Persistence	Mass score	Baryon score
1	3	1.0	0.966	0.680	45.59	2.796
0	3	1.0	0.966	0.679	54.19	2.822
2	3	1.0	0.960	0.678	60.70	2.838
4	3	1.0	0.964	0.676	47.79	2.797
3	3	1.0	0.961	0.675	43.23	2.779

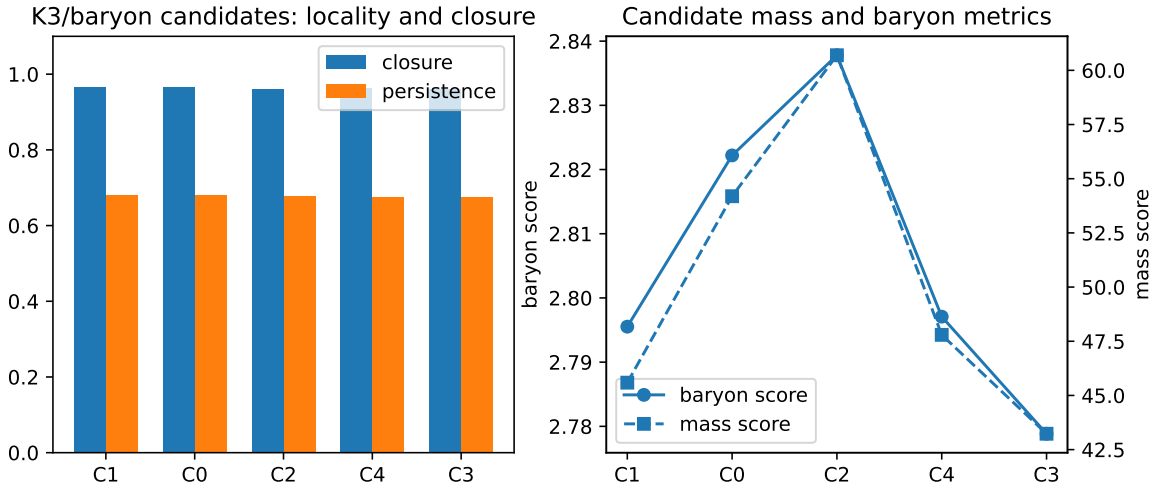

Figure 5: K3/baryon-like candidates. The open-token detector recovers five stable K3-centered candidates with $k3\_score = 1.0$, high closure, stable carrier support, and clustered baryon scores.

The result should be interpreted as a particle-like candidate result, not as a completed baryon mass spectrum. The claim is that the open-token registry carrier supports stable K3-centered localized excitations with baryon-like detector signatures.

8.2 Null-model audit for K3 candidates

As a first structural null audit, we asked how often random three-node supports form complete K_3 motifs in the recovered DAG-7 overlap graph. In the condensable non-universal substrate, 79,422 of 325,500 possible triples are K_3 motifs, giving $p(K_3) = 0.244$. The probability that five independently sampled triples are all K_3 is therefore $0.244^5 = 8.65 \times 10^{-4}$; a Monte Carlo audit over 200,000 five-triple draws gave a smoothed empirical probability $p_{\text{emp}} = 7.45 \times 10^{-4}$.

8.3 I-cage/lepton-like precursor

The I-cage experiment is more tentative. The detector identified a localized cage-overlap candidate with closure 1.0, carrier support 2, locality near 0.91, and cage/lepton score approximately 0.782. However, the strict count of closed localized cage leptons was zero. Therefore, the present manuscript treats this result as an I-cage/lepton-like precursor rather than as a closed lepton analogue (Fig. 6).

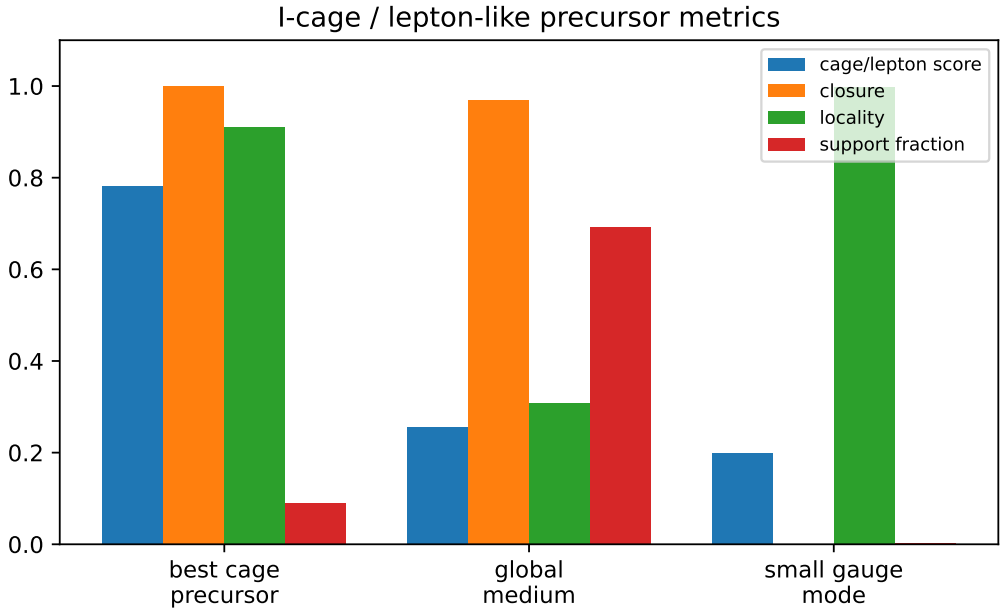

Figure 6: I-cage/lepton-like precursor metrics. The best cage-overlap candidate is localized and high scoring, but strict closed localized cage-lepton criteria are not yet met.

This negative boundary is useful. The mature carrier clearly supports interface-enabled condensation and K3-centered baryon-like candidates, but a fully closed lepton-like I-cage requires either a sharper detector, a more constrained initialization, or additional dynamical rules.

9 From carrier grammar to particle-like excitation

The mature-carrier and particle results combine into a single object ontology (Fig. 7). The DAG-7 registry supplies a finite type grammar. DAG-309 carriers embed the full grammar in lineage history. The S–I–G mediation tensor provides the functional invariant. Open-token dynamics supply repeated lineage-distinct instances. Particle-like structures are then stable excitation patterns over this carrier population, not separate primitive objects.

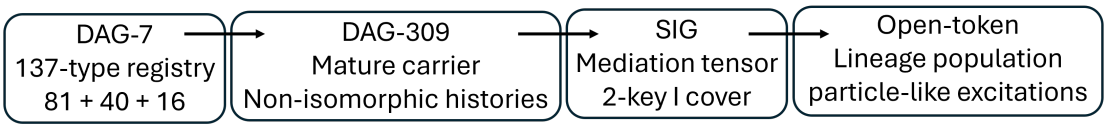

Figure 7: Conceptual pipeline from finite type grammar to open-token particle candidates. The closed distinction engine discovers a reusable registry grammar; mature carriers embed the full grammar; open-token dynamics supply lineage multiplicity and support particle-like excitations.

10 Discussion

10.1 Carrier history is not the physics

The mature-carrier analysis separates passive historical embedding from active typed mediation. Eight non-isomorphic DAG-309 carriers produce different merge histories, but the same condensable S–I–G mediation tensor. Dynamics are invariant across carrier history to the tested resolution. This suggests that the registry's functional physics resides in typed mediation coverage, not in the precise passive merge tree.

10.2 Interface function is distributed

The I-sector does not behave like a set of fragile active sites. Individual I-node identity is not essential. Instead, the interface sector is a distributed coverage code over the S–G conflict graph. The two complementary 19-node half-covers provide redundancy and explain why small I-node knockouts are neutral while coverage loss is damaging.

10.3 Type closure solves the scale problem

The distinction engine is closed as a type quotient, not as a token universe. This is essential. A finite type grammar can generate an open population of lineage-distinct tokens. The type-guarded open-token engine preserves the canonical 137 DAG-7 registry exactly while allowing token multiplicity. This permits a universe-scale population of registry instances without destroying the finite local grammar.

10.4 Particle-like results and limitations

The baryon-like K3 result is the strongest particle-like result in the present paper. Five stable K3-centered candidates are detected with perfect K3 score, high closure, fixed carrier support, and consistent baryon metrics. The I-cage/lepton-like result is suggestive but incomplete. We therefore avoid claiming a full particle spectrum.

Several limitations remain. First, these are simulations within the DE/RMR formalism and do not by themselves establish physical ontology. Second, the particle detector is heuristic and should be replaced by prospective locked tests. Third, the lepton-like I-cage result requires further refinement.

11 Conclusion

The mature-carrier and open-token particle analyses support a coherent object ontology for the distinction-engine registry. The canonical 137-object DAG-7 registry provides a reusable local type grammar. Minimal DAG-309 carriers embed the full registry in non-isomorphic histories while preserving a common typed mediation tensor. Interface-enabled condensation is invariant across carrier history and depends on complete I-mediated coverage of the S–G conflict graph. The type-guarded open-token engine preserves the canonical 137-type layer while allowing unbounded lineage-distinct multiplicity. Within this open-token setting, stable K3/baryon-like candidates appear, while I-cage/lepton-like structures appear as incomplete but suggestive precursors.

The results therefore support a staged object ontology. The present experiments recover stable K3-centered baryon-like cores in an open-token carrier population and identify I-cage/lepton-like precursors, but they do not yet recover neutral composite objects. This pattern is consistent with an early plasma-like excitation regime. The next natural test is a recombination-style detector for bound K3–I-cage composites.

Acknowledgments

The author acknowledges the role of large language models in code development and manuscript drafting. Interpretations and final claims remain the responsibility of the author. The code is available here: `https://github.com/jrmerwin/distinction_engine_objects.git`

References

[1] J. Merwin. Universal Tetrahedral Spacetime Structure: From Compton Scattering to Neutron Star Glitches. *ai.viXra.org:2601.0036*, 2026.

[2] J. Merwin. Cross-Scale Evidence for Discrete Spacetime Structure. *ai.viXra.org:2601.0070*, 2026.

[3] J. Merwin. Geometric Origin of Fundamental Constants: Thirty Derivations from Discrete Relational Structure and the Substrate-Interface Duality. *ai.viXra.org:2601.0081*, 2026.

[4] J. Merwin. Temporal Necessity in Relational Mathematical Realism: A Godelian Argument Against the Block Universe. *ai.viXra.org:2602.0071*, 2026.

[5] J. Merwin. Quantum Indeterminacy as Gödelian Epistemic Limitation: Implications of Relational Mathematical Realism for Quantum Foundations. *ai.viXra.org:2602.0093*, 2026.

[6] J. Merwin. Relational Mathematical Realism III: The Hubble Tension as a Discrete Spacetime Measurement Artifact. *ai.viXra.org:2602.0116*, 2026.

[7] J. Merwin. Emergent Four-Force Dynamics from a Discrete 137-Element Registry: Gravity, Electromagnetism, Strong, and Weak Interactions via Causal Integer Lattice Simulation. *ai.viXra.org:2603.0003*, 2026.

[8] J. Merwin. Relational Mathematical Realism: Registry Architecture Predicts Lepton, Baryon, and Strange Baryon Mass Spectra. *ai.viXra.org:2603.0062*, 2026.

[9] J. Merwin. A Discrete CMB Angular Power Spectrum from a Causal Integer Graph: Zero Free Parameters, Two Acoustic Peaks, and a Convergence Prediction for Planck 2018. *ai.viXra.org:2603.0064*, 2026.

[10] J. Merwin. Thermodynamic Screening Corrections in Relational Mathematical Realism: Mass Predictions from Graph Topology and a Universal Screening Unit. *ai.viXra.org:2603.0072*, 2026.

[11] J. Merwin. A Closed Distinction Engine: Derivation of a 137-Object Registry, a (81, 40, 16) Partition, and a K9 Bedrock Collapse from Two Primitives. *ai.viXra.org:2604.0072*, 2026.

[12] K. G. Wilson. Confinement of quarks. *Physical Review D*, 10(8):2445–2459, 1974.

[13] S. Wolfram. *A New Kind of Science*. Wolfram Media, 2002.

[14] R. D. Sorkin. Causal sets: discrete gravity. In *Lectures on Quantum Gravity*, pages 305–327. Springer, 2003.

[15] M. Tegmark. The mathematical universe. *Foundations of Physics*, 38:101–150, 2008.